Tropical Intraseasonal Oscillations Appearing in a GFDL General Circulation Model and FGGE Data. Part I: Phase Propagation

Y. HAYASHI AND D. G. GOLDER

Geophysical Fluid Dynamics Laboratory/NOAA, Princeton University, Princeton NJ 08542

(Manuscript received 10 February 1986, in final form 20 June 1986)

ABSTRACT

Space–time spectrum and filter analyses are made of the tropical intraseasonal oscillations in the northern summer appearing in a GFDL 30-wavenumber spectral general circulation model and the FGGE IIIB data.

The model exhibits major and minor wavenumber 1 spectral peaks in the equatorial zonal velocity at eastward-moving periods of 40–50 and 25–30 days in agreement with the FGGE data. Both the 40–50 and 25–30 day oscillations are associated with a similar spatial structure. In particular, both of these oscillations exhibit a phase reversal between the 200 and 800 mb zonal velocities. They propagate eastward with a node near the dateline and an antinode in the western hemisphere. Their wave patterns take the form of an eastward-moving Kelvin mode near the equator and an eastward-moving Rossby mode away from the equator.

Both spectral peaks are also detectable in the model's precipitation, corresponding to those in the observed outgoing longwave radiation. The 40–50 and 25–30 day precipitation oscillations are in phase with the vertical velocity and propagate northeastward with major and minor antinodes in the eastern and western hemispheres, respectively.

The present results demonstrate that the intraseasonal oscillations can be simulated in a model without air–sea interactions and cloud-radiation feedbacks.

1. Introduction

Recently, there has been a renewed interest in the tropical 40–50 day oscillation found by Madden and Julian (1971). This oscillation has been interpreted as representing intraseasonal oscillations with time scales of 30–60 days. These oscillations modulate monsoon activity (Yasunari, 1980), although they explain only 10% of the total time variance of the zonal wind (Krishnamurti and Gadgil, 1985). Madden and Julian (1972) suggested that the 40–50 day oscillation takes the form of a planetary-scale, zonal-vertical cell that propagates eastward, presumably with eastward-propagating convective heating. Yasunari (1980, 1981) found that this oscillation propagates northward in the summer monsoon region and suggested that it is associated with local meridional-vertical circulations. Maruyama (1982) showed that this oscillation is, to some extent, associated with a standing wave oscillation as well as an eastward phase propagation. Anderson and Rosen (1983) showed that the 40–50 day oscillation is also detectable in the zonal mean zonal velocity. Goswami and Shukla (1984) found a 20–40 day oscillation in a zonally symmetric general circulation model. Lorenc (1984) and Krishnamurti et al. (1985) showed an eastward propagation of the intraseasonal divergence field, while Weickmann (1983) showed an eastward propagation of the intraseasonal outgoing longwave radiation, which is interpreted as a measure of convective activity. Murakami et al. (1984) studied the three-dimensional phase propagation and structure of the 40–50 day oscillation and concluded that its major energy source is the conversion of potential energy into kinetic energy.

Parker (1973) interpreted this oscillation as the theoretical equatorial Kelvin wave mode studied by Matsuno (1966), although the vertical scale of the low frequency Kelvin wave is unrealistically small in the absence of heating. Chang (1977) suggested that the observed vertical scale can be explained by the effect of strong viscosity even in the absence of heating. Yamagata and Hayashi (1984) demonstrated by modifying a two-dimensional linear response model of Gill (1980) that both the eastward-moving Kelvin mode and the westward-moving Rossby mode are excited to the east and west of a localized thermal forcing which is assumed to pulsate with a 40-day period. However, there is the possibility that the heating itself has a periodicity and a zonal phase propagation as a result of mutual interactions between large-scale waves and cumulus convection as in the wave-CISK theory (Hayashi, 1970; Lindzen, 1974), although as of yet there is no wave-CISK theory for intraseasonal oscillations. There is also the possibility that the intraseasonal oscillations result from interactions with the ocean or ground hydrology as suggested by dynamical models of Webster and Chou (1980) and Webster (1983).

In view of these studies, it is of importance to study the intraseasonal oscillations by the use of a general circulation model. For this purpose, these oscillations

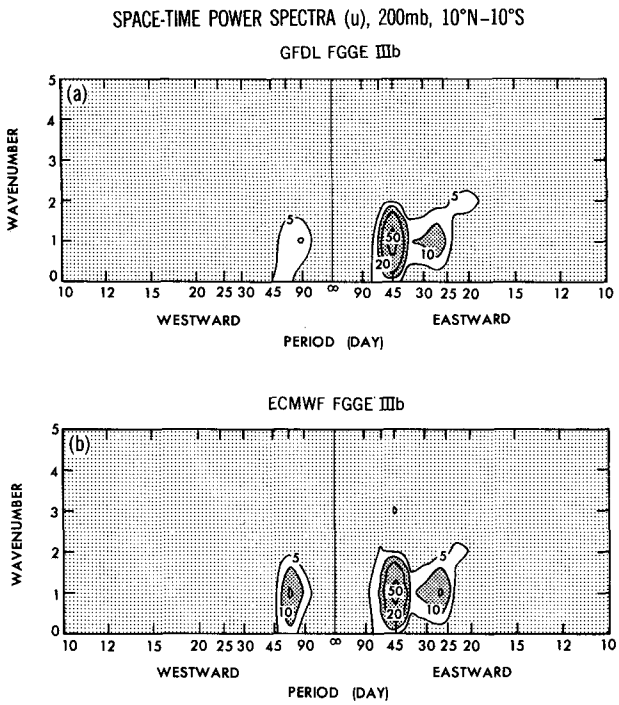

FIG. 1. Wavenumber–frequency distribution (200 mb, May–September) of the space–time power spectral density (10 $m^2 s^{-2}$ day) of zonal velocity averaged over 10°N–10°S. Dark shade: >10; light shade: <5. Contours under the light shade are not drawn. (a) GFDL FGGE IIIb data, (b) ECMWF FGGE IIIB data.

must be reasonably well simulated by a current model without air–sea interactions. It is then possible to examine whether convective heating associated with these oscillations is a local pulsation as in the linear response model or a traveling wave as in the wave-CISK theory. The model can also provide information on the detailed structure and energetics of these oscillations and can identify the roles that land and sea surfaces and condensational heating play by removing these effects from the model.

As the first step toward these goals, space–time spectrum and filter analyses have been made of the tropical intraseasonal oscillations appearing in GFDL general circulation models and the FGGE IIIb data. In the present paper (Part I), the spectral distribution, phase propagation and structure are examined. The detailed structure of these oscillations will be studied in Part II, which will be completed in the near future.

2. Space–time spectrum and filter analyses

a. Models and data

The models analyzed are 9-level GFDL spectral models with rhomboidal truncation at wavenumber 30 and 15 (hereafter referred to as R30 and R15) with the same viscosity coefficients. These models have latitudinal resolutions of 2.25° and 4.5°, respectively. Their physical processes include a moist convective adjustment, surface hydrology, a planetary boundary layer, radiation processes, orography and imposed annual cycles of insolation and climatological sea surface temperature and climatological cloudiness. Detailed descriptions of these models are given by Manabe et al. (1979) and Gordon and Stern (1982). For comparison, the same analyses have been made of the FGGE IIIb data (four-dimensional assimilation) processed by use of general circulation models with climatological sea surface temperatures at GFDL (see Ploshay et al., 1983) and those processed at the ECMWF (European Centre for Medium Range Weather Forecasts; see Bengtsson et al., 1982). The present paper concentrates on the results of the R30 model and the GFDL FGGE data in the northern summer (May–September). All references to the FGGE data will mean the GFDL FGGE data, unless otherwise noted. In order to gain sufficient frequency resolution from the short record, space–time spectra have been estimated by the maximum entropy method (see Hayashi, 1982) after the seasonal variations have been removed by subtracting 30-day means from once-daily data. Phase propagations have been visualized by the use of a recursive filter (see Murakami, 1979).

b. Zonal velocity and geopotential

Figure 1 compares the space–time power spectra of the zonal velocity (200 mb, 10°N–10°S average) based

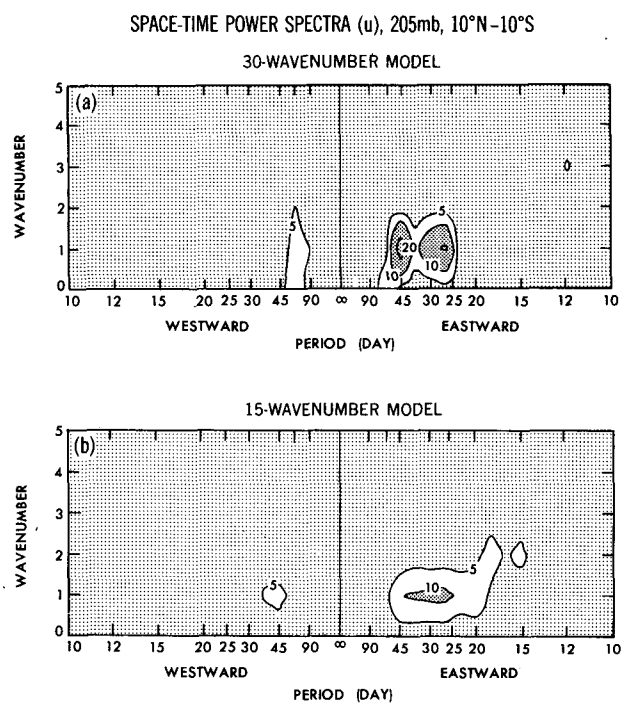

FIG. 2. As in Fig. 1 except for (a) R30 model and (b) R15 model at 205 mb.

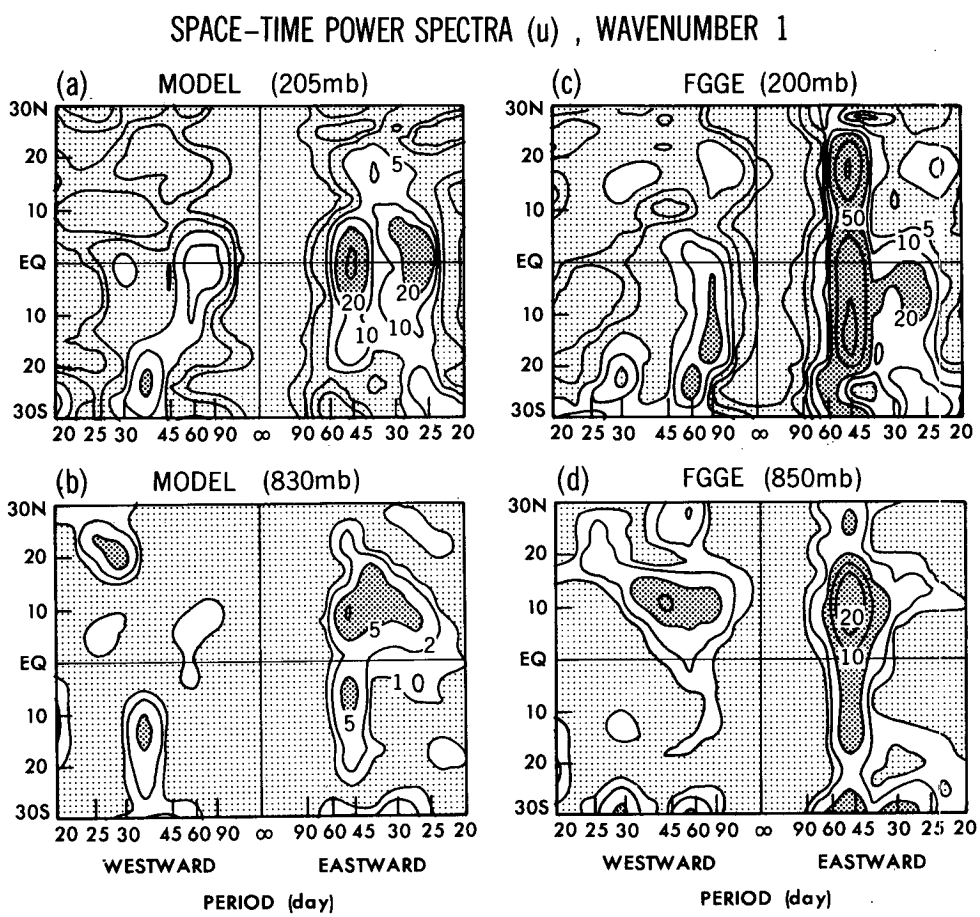

FIG. 3. Frequency–latitude distributions of space–time power spectral density (10 $m^2 s^{-2}$ day) of the zonal velocity (wavenumber 1) of the R30 model at (a) 205 mb and (b) 830 mb; and of FGGE at (c) 200 mb and (d) 850 mb. Contours at 1, 2, 5, 10, 20, 50, 100.

on the two sets of the FGGE IIIb data processed at GFDL and ECMWF. Both sets exhibit major and minor wavenumber 1 spectral peaks at eastward-moving periods of 40–50 and 25–30 days, respectively. This agreement assures that the FGGE intraseasonal oscillations do not crucially depend on the assimilation models and can essentially be considered as those observed. It should be mentioned that the space–time spectra of the ECMWF data calculated by Murakami (1982) and Nakazawa (1985a, Fig. 1; 1985b, Fig. 10) are overestimated by a factor of 4 due to a miscalculation (Nakazawa, personal communication, 1986). A 25–30 day peak has also been found in the observed tropical and subtropical cloud amounts (Takeda and Ikeyama, 1984; 1985).

Figure 2 compares the space–time power spectra of the zonal velocity (205 mb, 10°N–10°S average) of the R30 and R15 models. The R30 spectra exhibit major and minor wavenumber 1 peaks at eastward-moving periods of 40–50 and 25–30 days in agreement with the FGGE data, although the 40–50 day peak of the R30 model is about one-half of that of the FGGE data. However, in the R15 model (Fig. 2b), the relatively

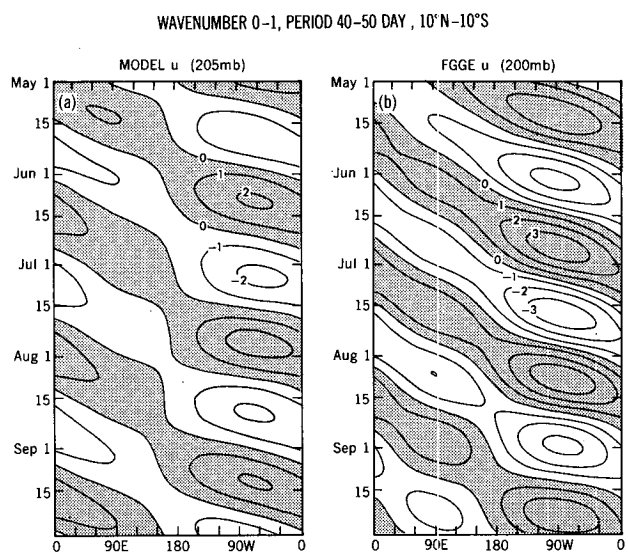

FIG. 4. Longitude–time distributions (10°N–10°S average) of the frequency-filtered (40–50 day) zonal velocity consisting of wavenumbers 0–1 components. (a) R30 model at 205 mb, (b) FGGE at 200 mb. Contour interval 1 m s^{-1}. Dark shade: >0.

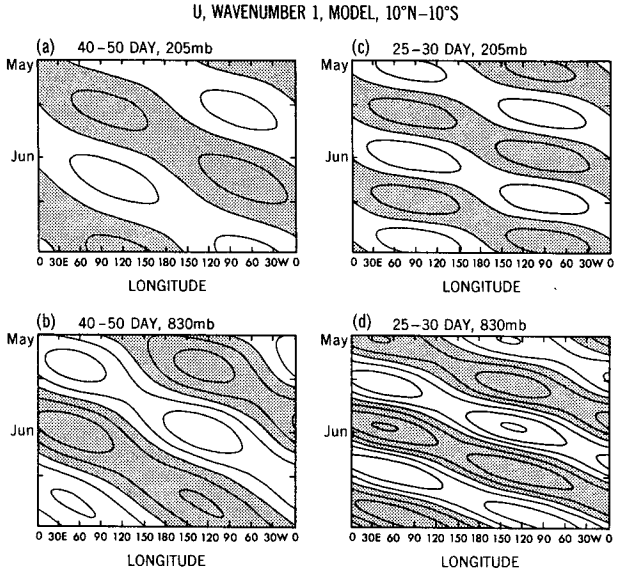

FIG. 5. Longitude–time distributions (10°N–10°S average) of the frequency-filtered zonal velocity of R30 model consisting of wavenumber 1 component only. With 40–50 day filter at (a) 205 mb and (b) 830 mb; with 25–30 day filter at (c) 205 mb and (d) 830 mb. Contour interval 1 m s^{-1}. Dark shade: >0.

large power spectra are found in a broad eastward-moving period range of 25–45 days, being consistent with a detailed analysis of the same R15 model based on 12 year integrations (Lau and Lau, personal communication, 1986). There is the possibility that the 40–50 day oscillation can occur more strongly in both R30 and R15 models when these models are somehow improved.

Figures 3a, b show the frequency–latitude distribution for the space–time power spectra of the zonal velocity (wavenumber 1) in the R30 model. At 205 mb (Fig. 3a), the 40–50 and 25–30 day peaks are centered over the equator. This is consistent with the interpretation (Parker, 1973) of the 40–50 day oscillation as the theoretical Kelvin mode of Matsuno (1966). However, at 830 mb (Fig. 3b), these peaks occur dominantly around 10°N, being contrary to the Kelvin mode. In the corresponding FGGE spectra (Figs. 3c, d), both spectral peaks are detectable. Moreover, the 40–50 day peak at 200 mb occurs over a broader range of latitudes than that of the R30 model.

In order to visualize how the 40–50 day oscillation propagates zonally, Fig. 4a, b shows the longitude–time sections of the R30 (205 mb) and FGGE (200 mb)

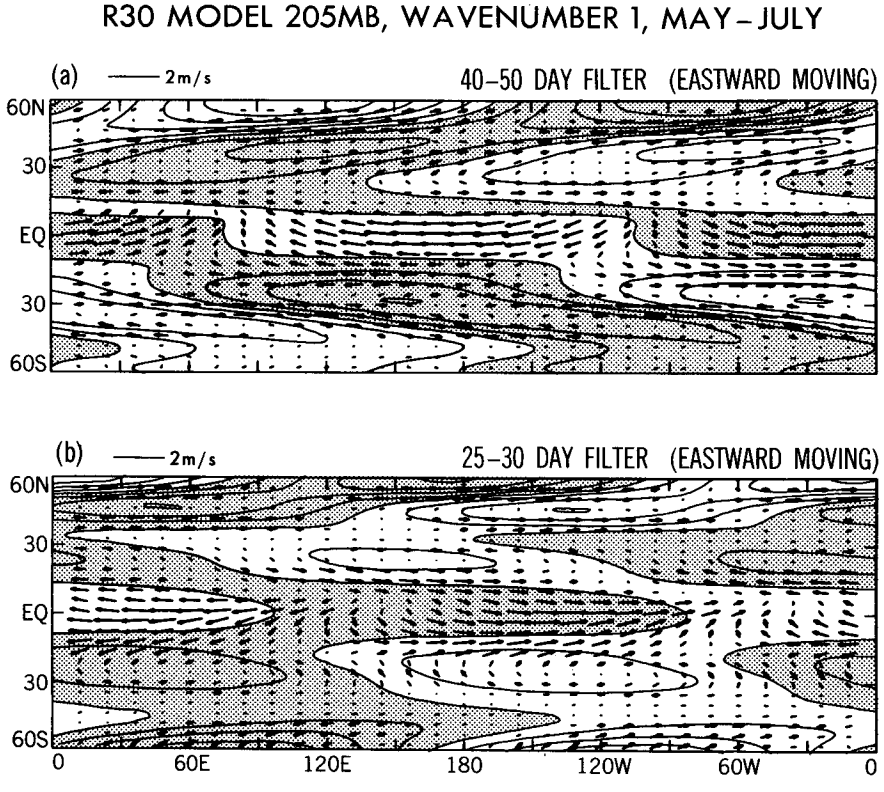

FIG. 6. Longitude–latitude distributions (R30 model, 205 mb) of the wavenumber 1 component of wind vectors and the geopotential height which are subjected to (a) 40–50 and (b) 25–30 day filters. These wave patterns are composited along the longitude–time phase line with eastward phase speeds of 10.3 and 16.8 m s^{-1}, respectively, during the period May through July. Contour intervals 2 m; shading indicates positive values.

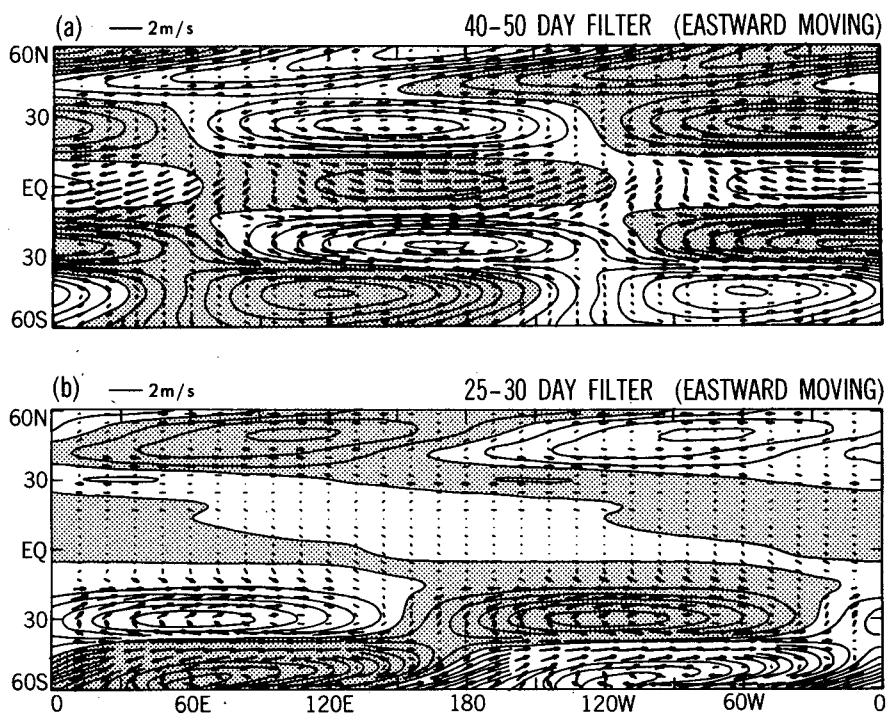

FIG. 7. As in Fig. 6 except for the FGGE data at 200 mb.

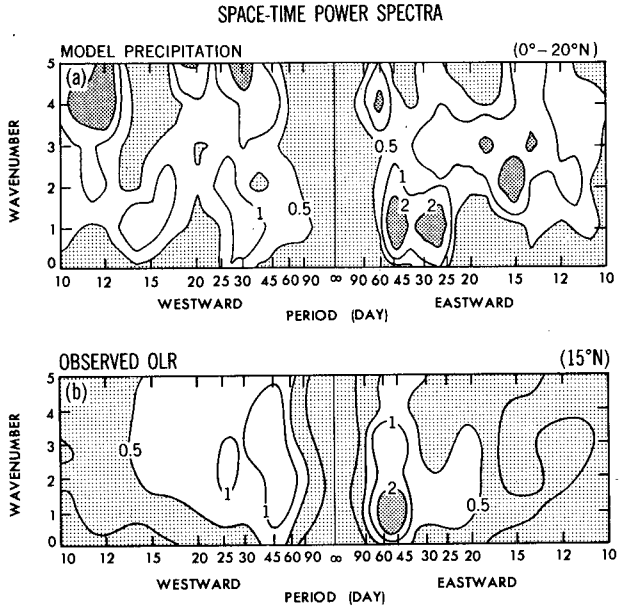

FIG. 8. (a) Wavenumber-frequency distribution of the space-time power spectral density (2.34×10^3 W^2 m^{-4} day) of latitudinally averaged (0–20°N) precipitational heating of R30 model. Contours 0.5, 1, 2. Dark shade: >2, light shade: <0.5. (b) As in (a) except for observed outgoing longwave radiation (15°N, May–September, 1975–77, 1979–83) (provided by Nakazawa, 1986). Units 10^2 W^2 m^{-4} day. Contours 0.2, 0.5, 1, 2. Dark shade: >2, light shade: <0.5.

zonal velocities (10°N–10°S average) consisting of wavenumber 0–1 components which have been subjected to a 40–50 day band-pass filter. The response function of this filter has been chosen in such a way that the amplitudes at 40- and 50-day periods are halved. These figures reveal some eastward phase propagation with one antinode in the western hemisphere and one node near the international dateline, although the node in the FGGE data is not as distinct as that found in the model. The antinode in the western hemisphere can be interpreted as a remote response of the zonal velocity to the thermal forcing which occurs in the eastern hemisphere, as will be shown in section 2c. The node is consistent with the spectral analysis (Maruyama, 1982) of observed data. This node appears in the linear response model of Yamagata and Hayashi (1984), although their model shows a westward phase propagation in the eastern hemisphere contrary to the present results. The R30 and FGGE 25–30 day oscillations are also associated with a node near the dateline and an antinode in the western hemisphere (not illustrated).

Figure 5 shows the longitude–time distributions at 205 and 830 mb of the 40–50 and 25–30 day zonal velocities (10°N–10°S average) of the R30 model consisting of wavenumber 1 only. It indicates that both these oscillations reverse their sign between the upper

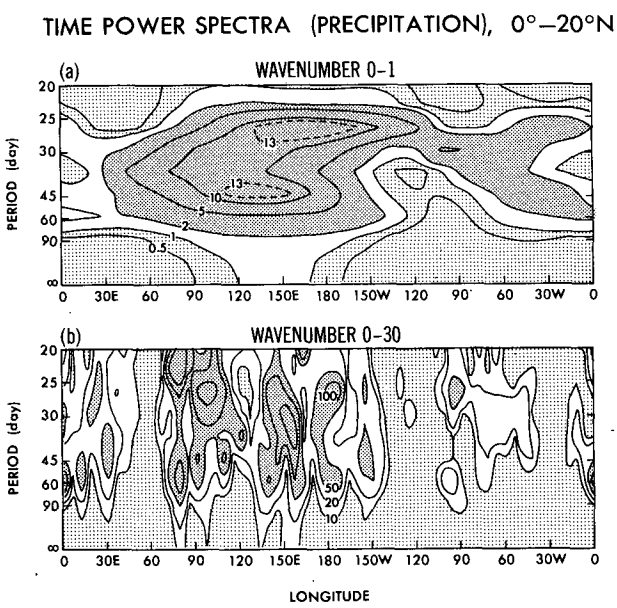

FIG. 9. Longitude–frequency distribution of the time power spectral density (2.34×10^3 W^2 m^{-4} day) of R30 precipitational heating (0–20°N average) consisting of wavenumbers (a) 0–1 and (b) 0–30. Contours 0.5, 1, 2, 5, 10, 20, 50, 100, 200, 500.

and lower levels. It should also be noted that, in the absence of the zonal mean oscillation, a pair of antinodes with opposite signs appear in the eastern and western hemispheres. These antinodes are due to the constructive interference between the eastward- and westward-moving components. In the presence of the zonal mean oscillation (Fig. 4a), one of the antinodes appears strongly due to the constructive interference between the wavenumber 0 and 1 components. The amplitude of the zonal mean and westward-moving components is not negligible against the amplitude of the eastward-moving component, although their power (amplitude square) is negligible against the power of the eastward-moving components. All these results from the R30 model agree with those of the FGGE data (not illustrated). The 40–50 day oscillation was also observed in the zonally averaged zonal velocity (Anderson and Rosen, 1983; Anderson et al., 1984).

Figure 6 shows the longitude–latitude distributions (R30 model, 205 mb) of the wavenumber 1 component of wind vectors and geopotential height contours which have been subjected to 40–50 and 25–30 day filters. These wave patterns have been composited along the longitude–time phase line with phase speeds of 10.3 and 16.8 m s^{-1}, respectively, during the period May through July. Near the equator both of these eastward-moving wave patterns resemble a Kelvin mode in that the wind vectors are nearly parallel to the equator and that the zonal velocity is in phase with the geopotential height. Away from the equator, these eastward-moving wave patterns resemble a Rossby mode in that the streamlines geostrophically follow the geopotential height contours and the zonal velocities reverse their direction with latitude. These features are also found in the FGGE data (Fig. 7), although the Kelvin mode component is very weak for the 25–30 day oscillations. The appearance of the Rossby mode pattern is consistent with the linear response model of Yamagata and Hayashi (1984), although their Rossby mode pattern moves westward.

c. *Precipitation and vertical velocity*

Figure 8a shows the space–time spectra of the R30 precipitational heating which is averaged over 0°–20°N. The 40–50 and 25–30 day peaks are clearly detectable corresponding to the wind spectra (Fig. 2a). Since precipitation is not available from the current FGGE IIIb data, corresponding space–time spectra of the observed outgoing longwave radiation (15°N, May–September) based on an 8-yr data set are presented (provided by Nakazawa, personal communication, 1986) in Fig. 8b. These spectra resemble the R30 precipitation spectra, although the observed OLR does not distinctly indicate a 25–30 day peak. The dominance of the eastward-moving component is consistent with the eastward propagation of intraseasonal OLR observed by Weickmann (1983), Weickmann et al. (1985), Lau and Chan (1985) and Knutson et al. (1986).

Figure 9a shows the longitude–frequency distribution of the time power spectral density of the R30 precipitation (0°–20°N average) consisting of wavenum-

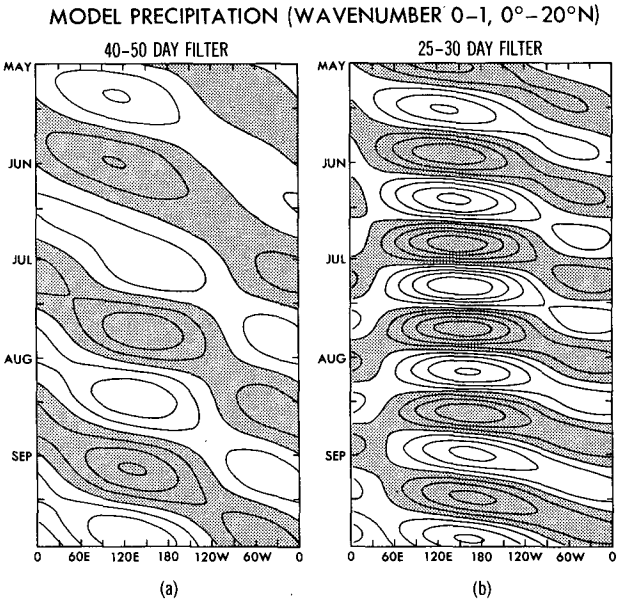

FIG. 10. Longitude–time distribution (0–20°N average) of R30 precipitational heating consisting of wavenumbers 0 and 1 subject to (a) 40–50 and (b) 25–30 day filters. Contour interval 4.8 W m^{-2}. Dark shade: >0.

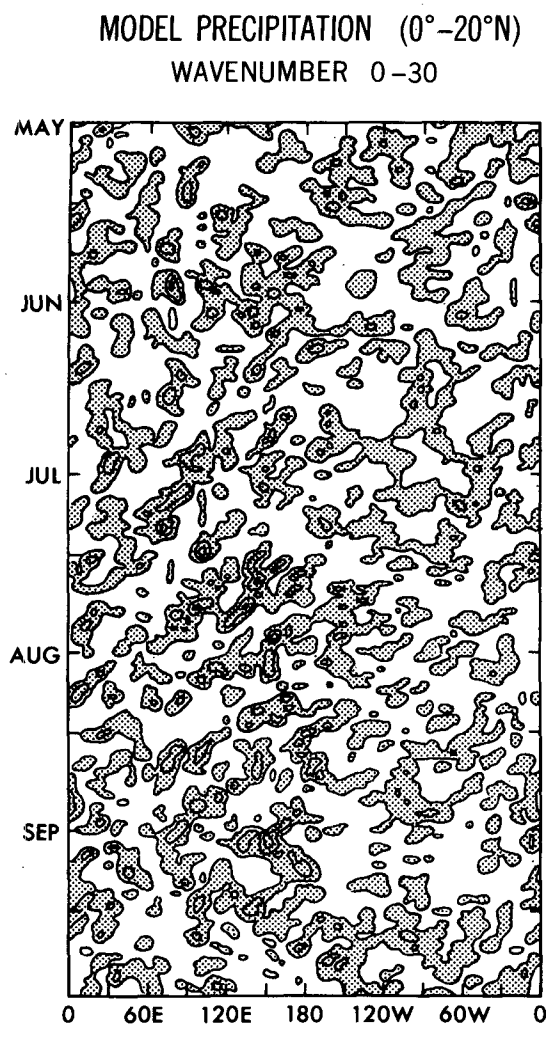

FIG. 11. As in Fig. 10 except for wavenumbers 0–30. Thirty-day means are subtracted without using time filters. Contour interval 2.4 W m^{-2}. Dark shade: >0. Negative contours are not drawn.

bers 0–1. The 40–50 day peak occurs primarily between 90°E and 180°, while the 25–30 day peak occurs primarily between 120°E and 120°W. These peaks are also detectable between 60°W and 0° longitudes. On the other hand, Fig. 9b shows the time spectra of precipitation consisting of all the wavenumbers (0–30). It is seen that both the 40–50 and 25–30 day precipitations are also associated with smaller scales.

Figures 10a, b show the longitude–time distributions (0°–20°N average) of the R30 precipitation consisting of wavenumber 0 and 1, which have been subjected to 40–50 and 25–30 day filters. These figures reveal eastward phase propagations with major and minor antinodes in the eastern and western hemispheres, respectively. These antinodes are probably related to the distribution of the sea surface temperature. Figure 11 is the same as Fig. 10 except that all the wavenumbers (0–30) of the model data are retained and 30 day means are subtracted without using time filters. Without space–time filtering, the eastward phase propagation is very difficult to detect due to the presence of small-scale noise.

Figures 12a, b show the time–latitude distributions (90°E–180° average) of the filtered R30 precipitation (wavenumber 1, periods 40–50 and 25–30 days). Both oscillations propagate with the phase velocity of about 1° per day in the Northern Hemisphere. This result is consistent with the northward propagation of observed cloudiness (Yasunari, 1980, 1981) and OLR (Knutson et al., 1986). It should be noted that both the 40–50 and 25–30 day wavenumber 1 components of precipitation are associated with a much shorter meridional scale than their zonal scale.

Figure 13 shows the time–latitude distributions (90°E–180° average) of the wavenumber 1 component of R30 (830 mb) and FGGE (850 mb) vertical velocities which have been subjected to 40–50 and 25–30 day filters. Both 40–50 and 25–30 day oscillations propagate northward with a phase velocity of about 1° per day in the Northern Hemisphere and are in phase with the precipitation. It should be noted that these wavenumber-1 vertical velocities are associated with a much shorter meridional scale than their zonal scale. The short meridional scale of divergence is hardly detectable in the FGGE velocity potential (Lorenc, 1984; Krishnamurti et al., 1985), which acts like a two-dimensional smoother.

3. Conclusions

The present paper (Part I) has isolated the tropical 40–50 and 25–30 day oscillations in the northern summer appearing in a general circulation model and the FGGE IIIb data processed at GFDL and ECMWF. The conclusions are summarized as follows:

1) The 30-wavenumber (R30) model exhibits major and minor wavenumber-1 peaks in the equatorial zonal velocity at eastward-moving periods of 40–50 and 25–30 days in agreement with the FGGE data, although the model's 40–50 day peak is associated with half of the power of the two sets of FGGE data. In the 15-wavenumber (R15) model, intraseasonal oscillations occur in a broad eastward period range of 25–45 days.

2) The R30 and FGGE 40–50 and 25–30 day zonal velocities propagate eastward with a node near the international dateline and an antinode in the western hemisphere. Both 40–50 and 25–30 day oscillations are associated with a similar three-dimensional structure. They reverse their sign between the 200 and 800 mb levels. Their wave patterns take the form of an eastward-moving Kelvin mode near the equator and an eastward-moving Rossby mode away from the equator.

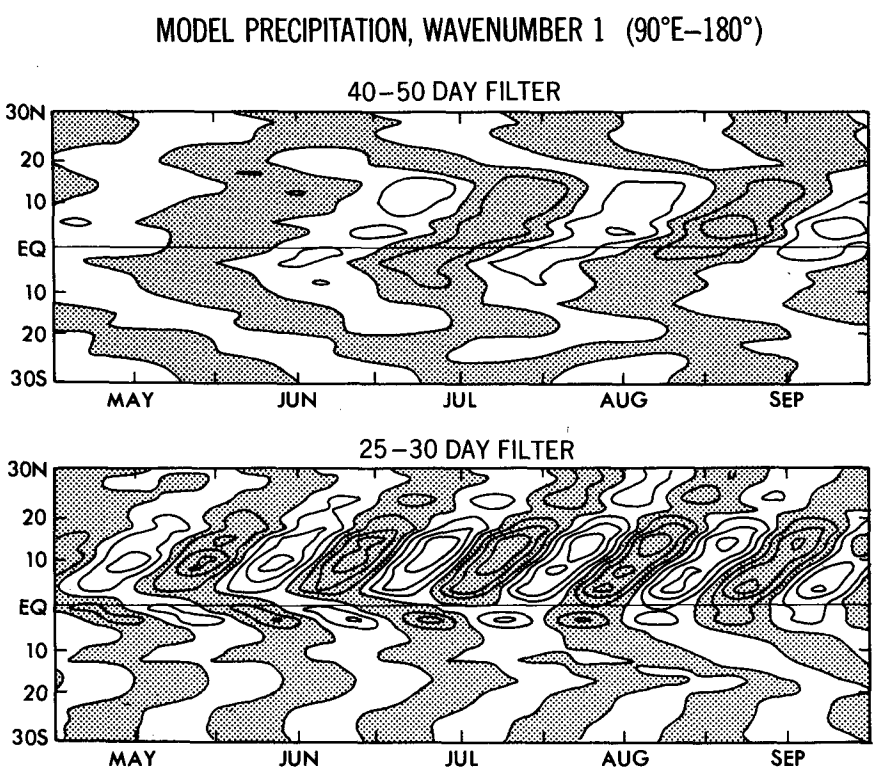

FIG. 12. Time–latitude distribution of the wavenumber 1 component (90°E–180° average) of R30 precipitational heating subject to (a) 40–50 and (b) 25–30 day filters. Contour interval 9.7 W m^{-2}. Dark shade: >0.

3) Both spectral peaks are detectable in the R30 precipitation, corresponding to those in the observed outgoing longwave radiation. The 40–50 and 25–30 day precipitations propagate eastward with a major and a minor antinode in the eastern and western hemispheres and are in phase with the vertical velocity. The wavenumber 1 precipitation and vertical velocity oscillations are associated with a much shorter meridional scale than their zonal scale and propagate northward in the Northern Hemisphere with a phase velocity of about 1° per day.

The present results have demonstrated that the intraseasonal oscillations can be simulated without air–sea interactions and cloud-radiation feedbacks. Although the present analysis is based on a May–September period, the 40–50 and 25–30 day spectral peaks are also clearly detectable in the zonal velocity and precipitation of the R30 model over one whole year, as illustrated in the Appendix (Fig. 14). It is unlikely that the R30 model's 40–50 day oscillation is extremely weaker than that observed over many years. It is also unlikely that the model's intraseasonal oscillations are associated with strong year-to-year variability in the tropics, since the model's sea surface temperature is not associated with interannual variability. It has been confirmed (not illustrated) that the 40–50 and 25–30 day spectral peaks are also detectable in a conventional grid model with 2.4° resolutions (Manabe et al., 1974), although these peaks were not resolved in the space–time spectral analysis of Hayashi (1974; Fig. 8a) due to the low spectral resolution in the analysis. It is somewhat puzzling that the R15 model is not capable of reproducing the dominant 40–50 day oscillation over the 25–30 day oscillation in spite of the similarity in their three-dimensional structure. There is the possibility that the 40–50 day oscillation can occur more strongly in both R30 and R15 models, when the parameterization of convection, the vertical resolution and physics of the boundary layer are improved.

The present results indicate that the Kelvin–Rossby mode patterns propagate eastward around the earth. This is contrary to the linear response model of Yamagata and Hayashi (1984) which is associated with eastward Kelvin and westward Rossby phase propagations to the east and west of the local pulsation of thermal forcing, although the appearance of the Rossby mode pattern and the nodes is consistent with their model. The eastward propagation of the Rossby mode pattern strongly supports the eastward phase propagation of thermal forcing, since unforced Rossby modes are associated with westward phase velocity relative to the basic flow.

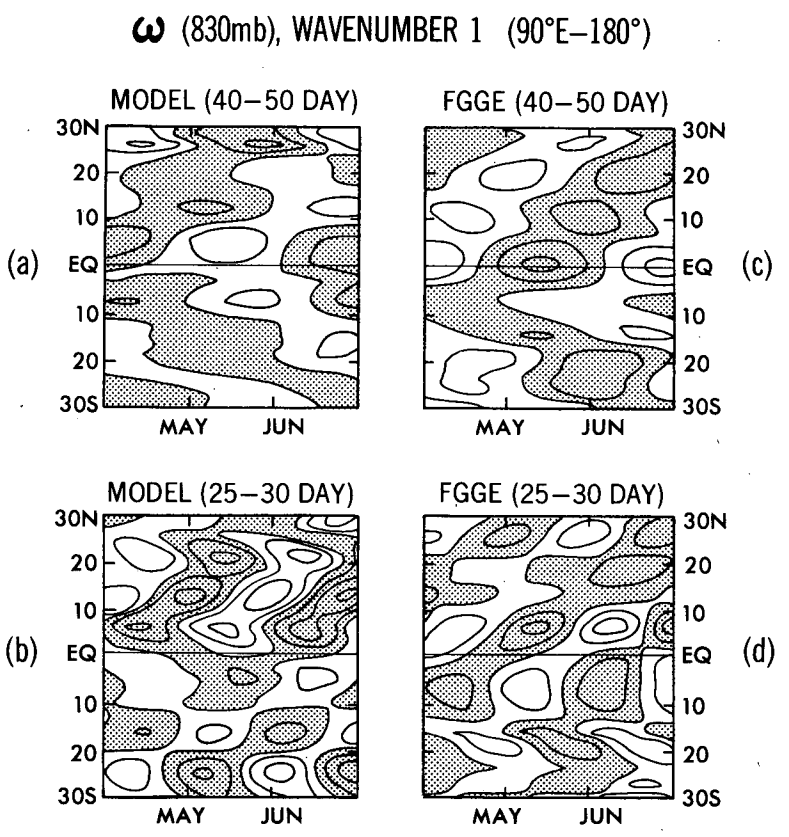

FIG. 13. Time–latitude distributions (90°E–180° average) of the wavenumber 1 component of vertical pressure velocity of R30 model (830 mb) subjected to (a) 40–50 and (b) 25–30 day filters; and of FGGE (850 mb) subjected to (c) 40–50 and (d) 25–30 day filters. Contour interval 2×10^{-11} Pa s^{-1}. Dark shade denotes downward velocity.

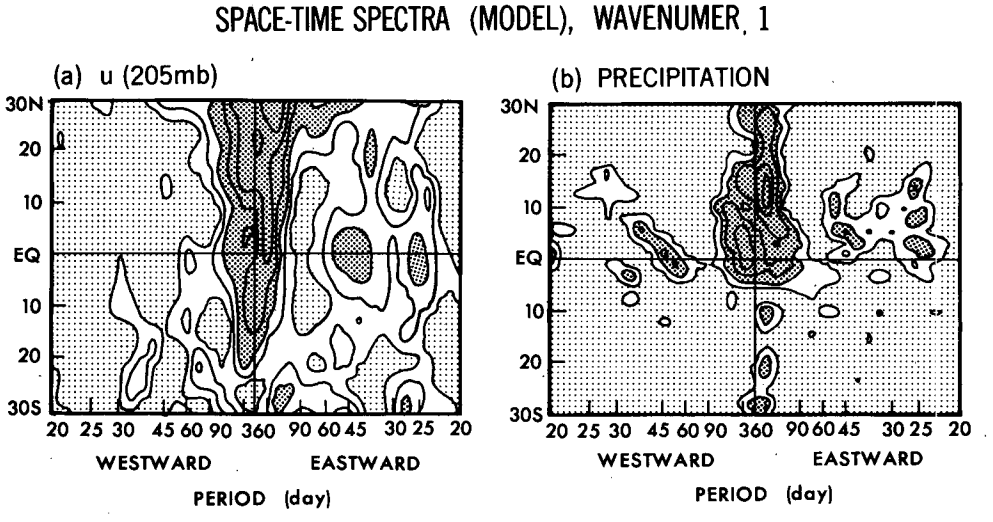

FIG. 14. Frequency–latitude distributions (R30 model; one whole year) of space–time power spectral density (wavenumber 1) of the (a) 205 mb zonal velocity and (b) precipitational heating. Seasonal variations are not filtered out. Contours 5, 10, 20, 50, 100. Units 10 m^2 s^{-2} day and 2.34×10^3 W^2 m^{-4} day. Light shade: <5.

The 40–50 and 25–30 day periodicities and northeastward phase propagation of the precipitation may be due to some mutual interactions between the waves and convective heating. In addition, some selective response of winds to red noise thermal forcing may help in reducing low-frequency variations in the winds. It is of interest to examine whether both 40–50 and 25–30 day oscillations will appear in a model without a zonal variation in the surface condition as demonstrated (Hayashi and Golder, 1978) for the 15-day stratospheric Kelvin wave.

Acknowledgments. The authors are grateful to Drs. S. Manabe, H. Kida, N. C. Lau, T. R. Knutson, I. M. Held and R. T. Pierrehumbert for their appropriate comments on the original manuscript and to Mr. T. Nakazawa for providing the OLR spectra. Thanks are extended to Mr. P. Tunison for the drafting of the figures.

APPENDIX

Space–Time Spectra of 1-Yr Data

In order to confirm that both 40–50 and 25–30 day spectral peaks appear in 1-yr data without eliminating the seasonal variations, Fig. 14 shows the frequency–latitude distributions (one whole year) of the space–time power spectral density (wavenumber 1) of the 205 mb zonal velocity and precipitation in the R30 model.

REFERENCES

Anderson, J. R., and R. D. Rosen, 1983: The latitude–height structure of 40–50 day variations in atmospheric angular momentum. *J. Atmos. Sci.*, **40**, 1584–1591.

——, D. E. Stevens and P. R. Julian, 1984: Temporal variations of the tropical 40–50 day oscillation. *Mon. Wea. Rev.*, **112**, 2431–2438.

Bengtsson, L., M. Kanamitsu, P. Kallberg and S. Uppals, 1982: FGGE four-dimensional data assimilation at ECMWF. *Bull. Amer. Meteor. Soc.*, **63**, 29–43.

Chang, C. P., 1977: Viscous internal gravity waves and low frequency oscillations in the tropics. *J. Atmos. Sci.*, **34**, 901–910.

Gill, A. E., 1980: Some simple solutions for heat-induced tropical circulations. *Quart. J. Roy. Meteor. Soc.*, **106**, 447–462.

Gordon, C. T., and W. F. Stern, 1982: A description of the GFDL global spectral model. *Mon. Wea. Rev.*, **110**, 625–644.

Goswami, B. N., and J. Shukla, 1984: Quasi-periodic oscillations in a symmetric general circulation model. *J. Atmos. Sci.*, **41**, 20–37.

Hayashi, Y., 1970: A theory of large-scale equatorial waves generated by condensational heat and accelerating the zonal wind. *J. Meteor. Soc. Japan*, **48**, 140–160.

——, 1974: Spectral analysis of tropical disturbances appearing in a GFDL general circulation model. *J. Atmos. Sci.*, **31**, 180–218.

——, 1982: Space-time spectral analysis and its applications to atmospheric waves. *J. Meteor. Soc. Japan*, **60**, 156–171.

——, and D. G. Golder, 1978: The generation of equatorial transient planetary waves: Control experiments with a GFDL general circulation model. *J. Atmos. Sci.*, **35**, 2068–2082.

Knutson, T. R., K. M. Weickmann and J. E. Kutzbach, 1986: Global scale intraseasonal oscillations of outgoing longwave radiation and 250 mb zonal wind during Northern Hemisphere summer. *Mon. Wea. Rev.*, **114**, 605–623.

Krishnamurti, T. N., and S. Gadgil, 1985: On the structure of the 30–50 day mode over the globe during FGGE. *Tellus*, **37A**, 336–360.

——, P. K. Jayakumar, J. Sheng, N. Surgi and A. Kumar, 1985: Divergent circulations on the 30 to 50 day time scale. *J. Atmos. Sci.*, **42**, 364–375.

Lau, K. M., and P. H. Chan, 1985: Aspects of the 40–50 day oscillation during the northern winter as inferred from outgoing longwave radiation. *Mon. Wea. Rev.*, **113**, 1889–1909.

Lindzen, R. S., 1974: Wave-CISK in the tropics. *J. Atmos. Sci.*, **31**, 156–179.

Lorenc, A. C., 1984: The evolution of planetary scale 200 mb divergences during the FGGE year. *Quart. J. Roy. Meteor. Soc.*, **110**, 427–441.

Madden, R. A., and P. R. Julian, 1971: Detection of a 40–50 day oscillation in the zonal wind in the tropical Pacific. *J. Atmos. Sci.*, **28**, 702–708.

——, and ——, 1972: Description of global-scale circulation cells in the tropics with a 40–50 day period. *J. Atmos. Sci.*, **29**, 1109–1123.

Manabe, S., D. G. Hahn and J. L. Holloway, Jr., 1974: The seasonal variation of the tropical circulation as simulated by a global model of the atmosphere. *J. Atmos. Sci.*, **31**, 43–83.

——, —— and ——, 1979: Climate simulations with GFDL spectral models of the atmosphere: Effect of truncation. GARP Publ. Ser., No. 22, Vol. 1, 41–94.

Maruyama, T., 1982: Upper tropospheric zonal wind oscillation with a 30–50 day period over the equatorial western Pacific observed in cloud movement vectors. *J. Meteor. Soc. Japan*, **60**, 172–182.

Matsuno, T., 1966: Quasi-geostrophic motions in the equatorial area. *J. Meteor. Soc. Japan*, **44**, 25–43.

Murakami, M., 1979: Large-scale aspects of deep convective activity over the GATE area. *Mon. Wea. Rev.*, **107**, 994–1013.

Murakami, T., and T. Nakazawa, 1985a: Tropical 45 day oscillation during the 1979 Northern Hemisphere summer. *J. Atmos. Sci.*, **42**, 1107–1122.

——, and ——, 1985b: Transition from the Southern to Northern Hemisphere summer monsoon. *Mon. Wea. Rev.*, **113**, 1470–1486.

——, —— and J. He, 1984: On the 40–50 day oscillations during the 1979 Northern Hemisphere summer. Part I: Phase propagation. Part II: Heat and moisture budget. *J. Meteor. Soc. Japan*, **62**, 440–468, 469–484.

Nakazawa, T., 1986: Intraseasonal variations of OLR in the tropics during the FGGE year. *J. Meteor. Soc. Japan*, **64**, 17–34.

Parker, D. E., 1973: Equatorial Kelvin waves at 100 millibars. *Quart. J. Roy. Meteor. Soc.*, **99**, 116–129.

Ploshay, J., R. White and K. Miyakoda, 1983: FGGE III-b daily global analyses. Part I. NOAA Rep., ERL GFDL 1., U.S. Dept. of Commerce, 278 pp.

Takeda, T., and M. Ikeyama, 1984: Time variation of cloud amount with about 30-day period in the western North Pacific region. *J. Meteor. Soc. Japan*, **62**, 165–171.

——, and ——, 1985: Time variation of cloud amount with about 30-day period in the western Pacific region. *J. Meteor. Soc. Japan*, **63**, 997–1012.

Webster, P. J., 1983: Mechanisms of monsoon low frequency variability: Surface hydrological effects. *J. Atmos. Sci.*, **40**, 2110–2124.

——, and L. C. Chou, 1980: Low frequency transitions of a simple monsoon system. *J. Atmos. Sci.*, **37**, 368–382.

Weickmann, K. M., 1983: Intraseasonal circulation and outgoing longwave radiation modes during Northern Hemisphere winter. *Mon. Wea. Rev.*, **111**, 1838–1858.

——, G. R. Lussky and J. E. Kutzbach, 1985: A global-scale analysis of intraseasonal fluctuations of outgoing longwave radiation and 250 mb streamfunction during northern winter. *Mon. Wea. Rev.*, **113**, 941–961.

Yamagata, T., and Y. Hayashi, 1984: A simple diagnostic model for the 30–50 day oscillation in the tropics. *J. Meteor. Soc. Japan*, **62**, 709–717.

Yasunari, T., 1980: A quasi-stationary appearance of 30 to 40 day period in the cloudiness fluctuations during the summer monsoon over India. *J. Meteor. Soc. Japan*, **58**, 225–229.

——, 1981: Structure of an Indian summer monsoon system with around 40-day period. *J. Meteor. Soc. Japan*, **59**, 336–354.